Can Soot Primary Particle Size be Determined Using Laser-Induced Incandescence?

RANDY L. VANDER WAL,* THOMAS M. TICICH, and A. BROCK STEPHENS

NASA-Lewis Research Center, Cleveland, OH 44135, USA (R.L.V.W.) and Department of Chemistry, Centenary College of Louisiana, Shreveport, LA 71134, USA (T.M.T., A.B.S.)

Temporally resolved laser-induced incandescence (LII) signals are obtained from different size primary particles produced by the diffusion flames of methane, ethane, ethylene, and acetylene. These results represent the first direct comparison between primary particle sizes based on optical measurements and those directly measured through transmission electron microscopy (TEM). Analysis of the data at different detected wavelengths as suggested by theory reveals a nonmonotonic relation with primary particle size as measured by TEM. Two alternative measures of the temporal decay of the signal at a single detected wavelength reveal a correlation with primary particle size within soot aggregates produced by the different flames. Comparison between predicted primary particle size based on the calibrations using the temporal analysis of the LII signal and TEM measurements reveals agreement within the growth region (low axial heights) and very late in the oxidation region (high axial heights) within an ethylene gas-jet diffusion flame. Significant differences exist at intermediate positions. These differences are interpreted as representing the effects of cluster–cluster aggregation within the oxidation region.

INTRODUCTION

Soot surface growth rather than nucleation has been found to dominate soot mass yield [1–4]. Essential in characterizing the rate of soot growth and assessing theoretical models is the soot surface area. For example, soot mass growth proceeds via hydrogen abstraction creating a surface radical site in preparation for acetylene addition to the site (HACA mechanism) [5]. In such a process, the mass addition rate will depend upon total surface area in addition to the number of potential reactive sites [6].

Several parameters characterizing soot mass growth rate can be readily measured optically, such as soot volume fraction (f_v), velocity, and temperature. Optical measurements are advantageous because they are nonintrusive and take place in real time. Optical, *in situ* determination of primary particle size would further facilitate measuring soot mass growth and oxidation rates per unit surface area. The current methodology for primary particle size determination is through analysis of transmission electron microscopy (TEM) micrographs of thermophoretically sampled soot, an intrusive and time-intensive process [2–4].

Largely due to its high temporal and spatial resolution, laser-induced incandescence (LII) has advanced f_v measurements to a wide range of combustion processes. Theoretical models of LII predict that the temporal evolution of the signal after the excitation laser pulse is dependent upon primary particle size [7–11]. This is physically sensible given that the temporal evolution of the LII signal is dependent upon the cooling of the primary particles predominantly through conduction and convection, processes dependent upon surface area. Thus the work presented here seeks to explore the potential of LII for determining primary particle size. Given the number of assumptions utilized in present LII theoretical models regarding the physical and structural properties of the laser-heated soot [7–11], we adopted an empirical approach to seek a correlation between the temporal decay rate of the LII signal and primary particle size as determined from analysis of transmission electron micrographs of thermophoretically sampled soot.

EXPERIMENTAL

A variety of laminar gas-jet diffusion flames produced by different fuels and flow rates were used to produce a wide range of primary parti-

*Corresponding author. Address: NCMR c/o NASA-Lewis Research Center, M.S. 110-3, 21 000 Brookpark Rd., Cleveland, OH 44135.

COMBUSTION AND FLAME 116:291–296 (1999)

Published by Elsevier Science Inc.

0010-2180/99/$19.00
PII S0010-2180(98)00040-6

TABLE 1

Summary of Experimental Conditions and Primary Particle Sizes

Fuel	Flow Rate (sccm)	Axial Height (mm)	Primary Size (nm) TEM	Temperature (K)
Methane	350	50	14.2 ± 1.5	1750
Ethane	255	61	20.4 ± 1.9	1700
Ethylene	231	50	33.3 ± 3.2	1600
Acetylene	200	50	59.7 ± 3.9	1200

sccm = standard cubic centimeters per minute.

cle sizes. Table 1 lists the different fuels, flow conditions, sampling heights above the burner, primary particle sizes, and local temperatures for each of the four flames studied. The fuels, sampling heights, and flow conditions were chosen to produce soot at the same point in its growth history (near the maximum size) at similar local temperatures along the axial streamline. In all cases, these diffusion flames were over-ventilated with an air coflow rate of 42.3 slm. Flame temperatures were measured at the specified axial position by 300 μm bead diameter type R thermocouples employing rapid insertion [12] with subsequent radiation correction [13]. Each gas-jet diffusion flame was supported on a 10.5-mm i.d. nozzle surrounded by an air coflow through a 101-mm-diameter honeycomb. A chimney with windows for optical access served to stabilize the flame and provide shielding from room drafts.

Figure 1 illustrates the experimental equipment. The 1064-nm light from a pulsed 30-Hz Nd:YAG laser was formed into a 500-μm-wide sheet and directed through the flame. The laser sheet profile was determined through knife-edge profiling. The laser fluence of 0.25 J/cm^2 was selected to provide LII temporal profiles whose decay times were relatively invariant (within 10%) with small variations in laser fluence. Such fluence dependence curves have been presented elsewhere [14–16]. LII signals were relayed through a quartz optical fiber to a monochromator fitted with a photomultiplier tube (PMT) as detector. The signal collection system has a spectral bandwidth of 12 nm and a transverse spatial resolution of 1 millimeter. Time-resolved PMT signals were sampled using a 500-MHz digital oscilloscope which also coaveraged 200 individual temporal scans.

Thermophoretic sampling provided soot samples for TEM. Probe residence times within the flames ranged from 30 to 60 ms depending on the soot volume fraction. TEM grids with ultrathin substrates aided visualization of the sampled soot. TEM micrographs were analyzed for primary particle size using commercial image processing software.

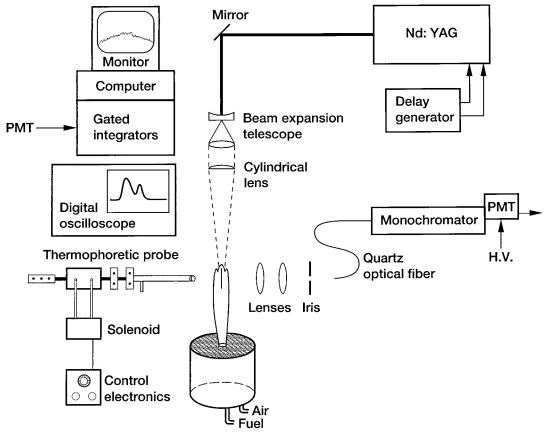

Fig. 1. Experimental schematic.

RESULTS AND DISCUSSION

Calibration Development

Figure 2 shows the time-resolved LII signals for three flames at the longest detection wavelength, 600 nm. Qualitatively similar data were obtained at shorter detection wavelengths, but the largest variation in the temporal evolution of the LII signal occurred at the longest detection wavelength.

Two analysis methods based on a theoretical model of the LII signal have been reported

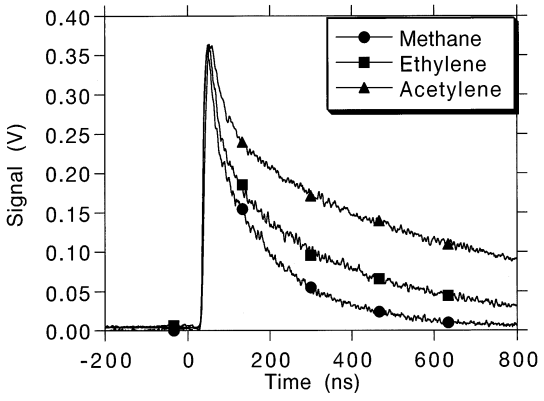

Fig. 2. Time-resolved LII signals produced by the different size primary particles in the different flames.

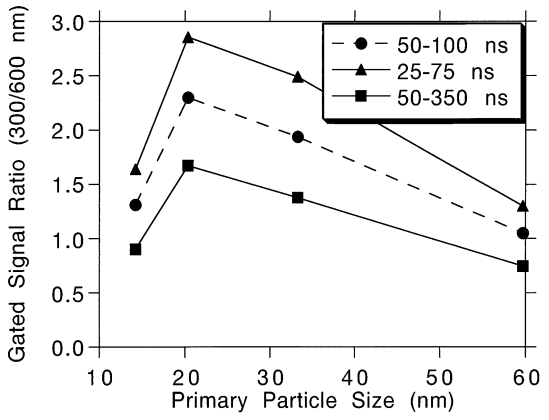

Fig. 3. Correlation between measured primary particle size and the signal intensity ratio at the indicated detected wavelengths for different signal integration times. The points along each curve represent measurements (with increasing primary particle size) from methane, ethane, ethylene, and acetylene, respectively.

recently for extracting primary particle size from LII data [10–11]. The first method uses the ratio of signal intensity (integrated over the same time delay and duration after the excitation laser pulse) at two detection wavelengths [10]. An advantage of this method, according to the theoretical model, is reduced sensitivity to differences in ambient flame temperature. We chose 300 nm and 600 nm as our analysis wavelengths to obtain as large a difference in observable decay times as allowed by the detection system. The averaging procedure for the method involved averaging 200 temporal decay scans at each wavelength separately using the digital oscilloscope. The ratio between the two data sets was formed from the integrated signals for the two data sets for the indicated time period. Reproducibility was generally within 10% between data sets from different days. Figure 3 shows the analysis of our data in this manner for several choices of time duration. In all cases, we obtained a nonmonotonic relationship between the ratio and primary particle size. Since these curves show two different primary particle sizes for a given signal ratio, they are clearly unacceptable as a calibration curve.

A second method of analysis, henceforth referred to as the gate ratio method, uses the same averaged temporal curve obtained at a single detection wavelength. The gate ratio is formed from signals integrated at two different delays after the excitation laser pulse. The results of this method of analysis applied to the time-resolved LII signals from the various-sized primary particles are shown in Fig. 4. The gate ratio in the figure uses delays of 0 ns and 300 ns both with a gate width of 50 ns. Other delays and gate widths also gave a monotonic relationship between gate ratio and primary particle size, but with a lower dynamic range.

Because this method uses a limited portion of the experimental data, we also sought a third method of analysis to utilize all the experimental data by fitting the signal decay to a mathematical function. Our analysis showed signifi-

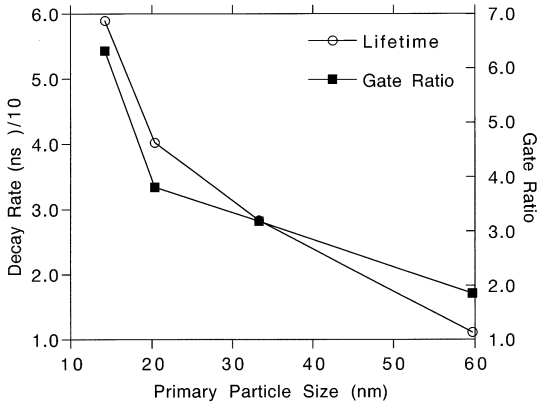

Fig. 4. Correlation between measured primary particle size and the second decay rate and gate ratio describing the temporally resolved LII signal. The points along each curve represent measurements (with increasing primary particle size) from methane, ethylene, ethane, and acetylene, respectively.

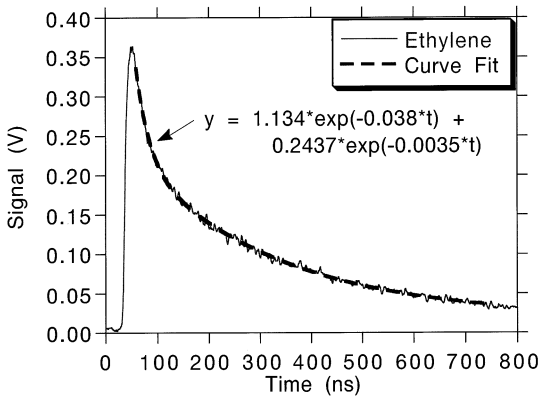

Fig. 5. Double-exponential curve fit to the LII signal from an ethylene flame (data also shown in Fig. 2).

cant disagreement between the time-resolved data and a single-exponential fit. Far better agreement was observed using a double-exponential fit, Signal(t) = $A\exp(-k_1 t)$ + $B\exp(-k_2 t)$, as shown in Fig. 5. The double-exponential curve fits were applied between data points where the signal intensity was 10% and 90% of the peak value yielding a correlation coefficient greater than 0.99 in all cases. The cooling process of the laser-heated soot reflects the concurrent contributions of radiation, conduction, and convection that vary with time after the excitation laser pulse [7–12]. Thus the dual time constants may reflect different timescales associated with the different cooling mechanisms. Using the fast decay rate did not give a monotonic relation with increasing primary particle size. Figure 4 plots the second decay rate value obtained by fitting the time-resolved LII signals for the various diffusion flames against their primary particle size. The dynamic range and monotonic relationship exhibited by the two analysis methods whose results are plotted in Fig. 4 give each potential as an empirical calibration curve for inferring primary particle size based on the temporal decay rate of the LII signal in other systems.

Application

Motivated by the need for measuring primary particle size to determine soot mass growth and oxidation rates per unit surface area [1–6], we tested the utility of the calibration curve for determining primary particle size. Time-resolved LII data were obtained at different heights above the burner along the axial streamline within the ethylene flame and subsequently fit to a double-exponential and also analyzed using the method of gate ratios. This ethylene flame has been widely studied and well-characterized [17]. The temperature along the axial streamline between 40 mm and 80 mm HAB (height above burner) varies by less than 10% (from 1600 K to 1700 K) [17]. Thus, differences in incandescence decay rates at various heights will be minimally affected by variations in flame temperature.

The trend exhibited in both calibration plots is similar to the predicted results published in Ref. 10. Although the acetylene point is consistent with this trend, it was not used because the lower flame temperature, which results from large radiative heat loss, will affect the cooling processes (see Table 1). The range of temperatures observed along the axial streamline in the ethylene flame, however, falls within the range of the three remaining calibration points. Given the uncertainty in the functional form of a curve-fit, line segments connecting the calibration points were used for interpolation. The ethane–ethylene segment was extrapolated to obtain primary particle sizes from points beyond the ethylene calibration point. Using the calibration curves presented in Fig. 4, the measured long-time decay rates and gate ratios at various heights in the ethylene flame were translated into primary particle sizes.

Figure 6 presents the results. In order to test the accuracy of the predictions, thermophoretic sampling measurements were performed followed by TEM microscopy and subsequent primary particle size analysis. These results are also plotted in Fig. 6. While good agreement is observed at 40, 45, 80, and 85 mm HAB, pronounced differences exist between 55 and 75 mm HAB where the values measured from the TEM micrographs are significantly below the predicted values. Note that the agreement observed at 50 mm HAB reflects its being used as a calibration point.

The deviations observed in the oxidation regions likely result from the aerosol process of cluster–cluster aggregation (CCA) [18]. Soon after the formation of aggregates within the growth region, clustering of aggregates can be-

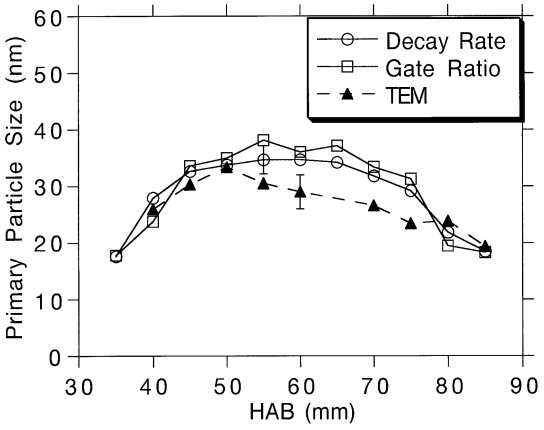

Fig. 6. Comparison between the predicted primary particle size based on the optical measurements and interpreted using the calibration curves in Fig. 4 and direct measurements from TEM micrographs.

gin. This process will continue to occur throughout the growth region and well into the oxidation region of the flame. TEM images of soot collected from the annular region of the flame show that as the aggregates cluster, they not only become larger but also more dense and compact [19, 20]. This is consistent with our own observations along the axial streamline. Figure 7 shows representative TEM images of soot aggregates collected at 40, 60, and 80 mm HAB. Although the effect is difficult to quantify, we do observe that the open branched-chain appearance of aggregates within the growth region does qualitatively change to a more densely packed, less open structure in the oxidation region. Such a structure could decrease the rate of cooling of individual primary particles (or fused units) through self-absorption of emitted thermal radiation and inhibition of conductive and convective cooling. Hence the optical measurement, which reflects the rate of temperature decrease of the laser-heated soot, would also be affected. Upon sufficient oxidation, the aggregates eventually crumble, so that the primary particles within the fragments return to a more open structure similar to that at their initial coalescence early within the growth region. At this stage, good agreement between the optical and TEM measurements would be expected, as observed at 80 mm HAB. It could be argued that the oxidation process itself could slow the rate of cooling of the laser-heated soot. Localized burning of the soot could contribute to locally elevated temperatures of the particles. Although optical pyrometry measures the temperature of soot particles whereas thermocou-

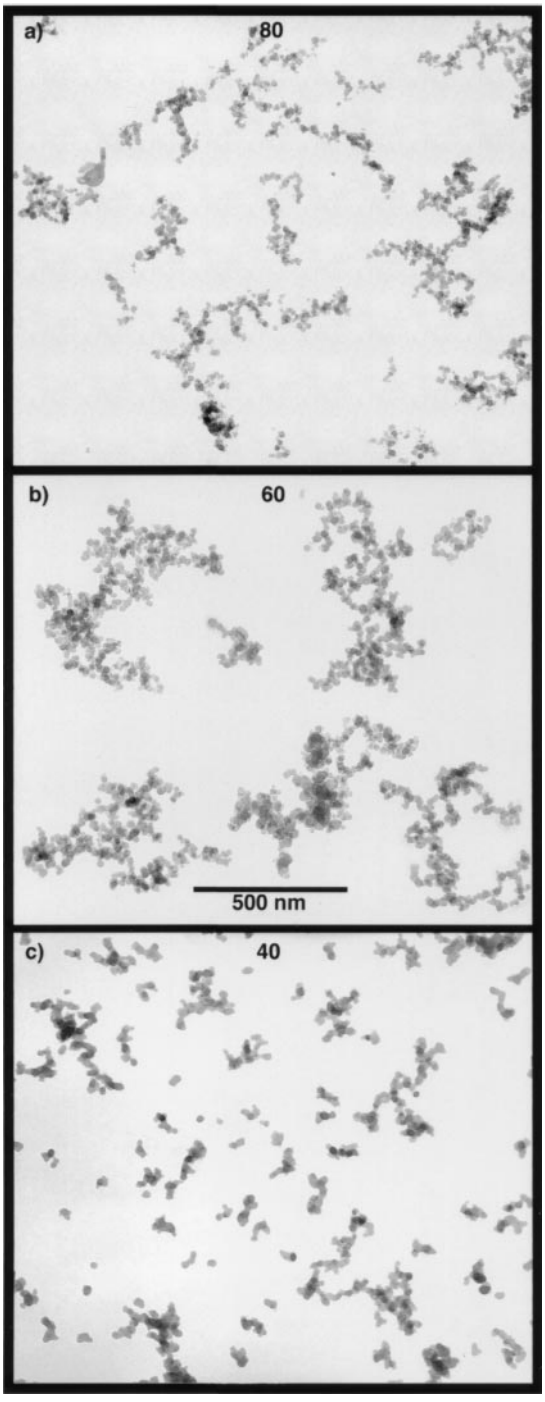

Fig. 7. TEM images of soot aggregates collected at (a) 80 mm, (b) 60 mm, and (c) 40 mm HAB.

ples measure the gas temperature, the two techniques are regarded as providing an equivalent measure of local temperature within measurement precision. Consistent with that perspective, we regard oxidation as a minor contributor to elevating particle temperature.

Another soot particle property that could affect the cooling process is the degree of primary particle connectivity. The degree of connectivity is a maximum at the peak of the soot growth region. Increasing primary particle connectivity would increase the effective primary particle size thus decreasing the cooling rate. Since our calibration points are at the peak of the growth region where the connectivity effects are maximum, this would underpredict primary particle sizes at other heights. The observed agreement between the predicted and experimental results within the soot growth region and the fact that the predicted results lie above the TEM measured values indicate that primary particle connectivity does not significantly impact the results presented here. The overprediction of the primary particle size relative to the TEM values within the oxidation region is also consistent with this postulate.

CONCLUSIONS

Our results suggest that LII can be used to predict primary particle size under certain conditions. Local flame temperature will affect the cooling rate of the particle and thus the optical signal. Therefore the flame temperature in the calibration system and the system to which it is applied must be similar in this empirical approach. CCA will also affect the cooling rate and the predicted primary particle sizes if it differs between the two systems. Particle–particle connectivity does not appear to be a significant factor in the results presented here.

These results represent the first direct comparison between primary particle sizes based on optical measurements and those directly measured through TEM. Predictions based on the temporal decay rate of the LII signal produce better agreement than those based on the gate ratio method.

This work was supported through NASA Contract NAS3-27186 with Nyma Inc. Professor Ticich and Mr. Brock Stephens gratefully acknowledge support through the Ohio Aerospace Institute ASEE summer faculty fellowship and accompanying student program.

REFERENCES

1. Harris, S. J., and Weiner, A. M., *Combust. Sci. Technol*. 38:75 (1984).
2. Megaridis, C. M., *Combust. Sci. Technol*. 66:1 (1989).
3. Sunderland, P. B., and Faeth, G. M., *Combust. Flame* 105:132 (1996).
4. Sunderland, P. B., Koylu, U. O., and Faeth, G. M., *Combust. Flame* 100:310 (1995).
5. Frenklach, M., and Wang, H., *Twenty-Third Symposium (International) on Combustion*, The Combustion Institute, Pittsburgh, 1990, p. 1559.
6. Howard, J. B., *Twenty-Third Symposium (International) on Combustion*, The Combustion Institute, Pittsburgh, 1990, p. 1107.
7. Melton, L. A., *Appl. Opt*. 23:2201 (1984).
8. Hofeldt, D. L. (1993). SAE Tech Paper 930079. Society of Automotive Engineers, Warrendale, PA.
9. Dasch, C. J., *Appl. Opt*. 23:2209 (1984).
10. Mewes, B., and Seitzman, J. M., *Appl. Opt*. 36:709 (1997).
11. Will, S., Schraml, S., and Leipertz, A., *Twenty-Sixth Symposium (International) on Combustion*, The Combustion Institute, Pittsburgh, 1996, p. 2277.
12. Eisner, D. A., and Rosner, D. E., *Combust. Flame* 61:153 (1985).
13. Smyth, K. C., Miller, J. H., Dorfman, R. C., Mallard, W. G., and Santoro, R. J., *Combust. Flame* 62:157 (1985).
14. Vander Wal, R. L., and Weiland, K. J., *Appl. Phys*. B59:445 (1994).
15. Ni, T., Pinson, J. A., Gupta, S., and Santoro, R. J., *Appl. Opt*. 34:7083 (1995).
16. Vander Wal, T. L., Ticich, T. M., and Stephens, A. B., *Appl. Phys. B* (In press).
17. Santoro, R. J., Yeh, T. T., Horvath, J. J. and Semerjian, H. G. *Combust. Sci. and Technol.* 53:89 (1987).
18. Puri, R., Richardson, T. F., Santoro, R. J. and Dobbins, R. A., *Combust. Flame* 92:320 (1993).
19. Dobbins, R. A., and Megaridis, C. M., *Langmuir* 3:254 (1987).
20. Koylu, U. O., Faeth, G. M., Farias, T. L., and Carvalho, M. G., *Combust. Flame* 100:621 (1995).

Received 23 October 1997; accepted 12 March 1998